Field-dependent magneto-optical Kerr effect spectroscopy applied to the magnetic component diagnosis of a rubrene/Ni system

Wen Li,[1,2] Michael Fronk,[1] Manfred Albrecht,[1,3] Mechthild Franke,[1] Dietrich R. T. Zahn,[1] and Georgeta Salvan[1,*]

[1]*Technische Universität Chemnitz, Institute of Physics, D-09107 Chemnitz, Germany*
[2]*Present address: Sino-European Institute of Aviation Engineering, Civil Aviation University of China, 300300 Tianjin, China*
[3]*Present address: University of Augsburg, Institute of Physics, D-86159 Augsburg, Germany*
[*]*salvan@physik.tu-chemnitz.de*

Abstract: Polar magneto-optical Kerr effect (MOKE) spectroscopy in the energy range from 1.75 eV to 5 eV at different magnetic field strength was applied to study Ni nanostructures formed on rubrene nanoislands. The magnetic hysteresis curves measured by MOKE change the shape depending on the photon energy and therefore deviate from those measured by superconducting quantum interference device (SQUID) magnetometry. Similar optical effects were previously observed in inorganic heterostructures. Our observations show that it correlates to the change in lineshape of the MOKE rotation and ellipticity spectra as a function of magnetic field strength. We show that this spectral dependence on magnetic field can be exploited to separate the contributions of two magnetic components to the magneto-optical spectra and hysteresis. The proposed model does not require the *a priori* knowledge of the (magneto-)optical constants of the heterostructure and its components.

©2014 Optical Society of America

OCIS codes: (160.3820) Magneto-optical materials; (240.0310) Thin films; (260.2130) Ellipsometry and polarimetry.

References and links

1. J. Ferré, P. Meyer, M. Nyvlt, S. Visnovsky, and D. Renard, "Magnetooptic depth sensitivity in a simple ultrathin film structure," J. Magn. Magn. Mater. **165**(1–3), 92–95 (1997).
2. Th. Herrmann, K. Lüdge, W. Richter, K. G. Georgarakis, P. Poulopoulos, R. Nünthel, J. Lindner, M. Wahl, and N. Esser, "Optical anisotropy and magneto-optical properties of Ni on preoxidized Cu(110)," Phys. Rev. B **73**, 134408 (2006).
3. G. R. Harp, D. Weller, T. A. Rabedeau, R. F. C. Farrow, and M. F. Toney, "Magneto-optical Kerr spectroscopy of a new chemically ordered alloy: Co_3Pt," Phys. Rev. Lett. **71**(15), 2493–2496 (1993).
4. M. Fronk, B. Bräuer, J. Kortus, O.G. Schmidt, D.R.T. Zahn, and G. Salvan, "Determination of the Voigt constant of phthalocyanines by magneto-optical Kerr-effect spectroscopy," Phys. Rev. B **79**, 235305 (2009).
5. B. Bräuer, M. Fronk, D. Lehmann, D. R. T. Zahn, and G. Salvan, "Magneto-optical Kerr effect spectroscopy--a sensitive tool for investigating the molecular orientation in organic semiconductor films," J. Phys. Chem. B **113**(45), 14957–14961 (2009).
6. K. Ishii and K. Ozawa, "Local-field-induced effective magnetic hysteresis of molecular magneto-optical effects in the visible region at room temperature: phthalocyanine thin films on ferromagnetic inorganic substrates," J. Phys. Chem. C **113**(43), 18897–18901 (2009).
7. T. Kitaguchi, T. Katayama, Y. Suzuki, N. Tsukane, and N. Koshizuka, "Organic dyes/co hybrid double layered film," Jpn. J. Appl. Phys. **30**(12A), 3377–3380 (1991).
8. W. Li, M. Fronk, H. Kupfer, S. Schulze, M. Hietschold, D. R. T. Zahn, and G. Salvan, "Aging of rubrene layers in Ni/rubrene heterostructures studied by magneto-optical Kerr effect spectroscopy," J. Am. Chem. Soc. **132**(16), 5687–5692 (2010).
9. L. F. Holiday and U. J. Gibson, "Improved longitudinal magneto-optic Kerr effect signal contrast from nanomagnets with dielectric coatings," Opt. Express **14**(26), 13007–13013 (2006).
10. N. Qureshi, H. Schmidt, and A. R. Hawkins, "Cavity enhancement of the magneto-optic Kerr effect for optical studies of magnetic nanostructures," Appl. Phys. Lett. **85**(3), 431–433 (2004).

#208434 - $15.00 USD Received 19 Mar 2014; revised 8 May 2014; accepted 24 Jun 2014; published 23 Jul 2014
(C) 2014 OSA

11. S. Visnovsky, K. Postava, and T. Yamaguchi, "Magneto-optic polar Kerr and Faraday effects in periodic multilayers," Opt. Express **9**(3), 158–171 (2001).
12. V. C. Sundar, J. Zaumseil, V. Podzorov, E. Menard, R. L. Willett, T. Someya, M. E. Gershenson, and J. A. Rogers, "Elastomeric transistor stamps: reversible probing of charge transport in organic crystals," Science **303**(5664), 1644–1646 (2004).
13. V. A. Dediu, L. E. Hueso, I. Bergenti, and C. Taliani, "Spin routes in organic semiconductors," Nat. Mater. **8**(9), 707–716 (2009).
14. D. Käfer and G. Witte, "Growth of crystalline rubrene films with enhanced stability," Phys. Chem. Chem. Phys. **7**(15), 2850–2853 (2005).
15. P. R. Ribič and G. Bratina, "Initial stages of growth of organic semiconductors on vicinal (0 0 0 1) sapphire surfaces," Surf. Sci. **602**(7), 1368–1375 (2008).
16. K. Postava, D. Hrabovský, O. Životský, J. Pištora, N. Dix, R. Muralidharan, J. M. Caicedo, F. Sánchez, and J. Fontcuberta, "Magneto-optic material selectivity in self-assembled $BiFeO_3$–$CoFe_2O_4$ biferroic nanostructures," J. Appl. Phys. **105**, 07C124 (2009).
17. J. Hwang, A. Wan, and A. Kahn, "Energetics of metal–organic interfaces: New experiments and assessment of the field," Mater. Sci. Eng. **4**(1–2), 1–31 (2009).
18. G. C. Papaefthymiou, "Nanoparticle magnetism," Nano Today **4**(5), 438–447 (2009).
19. W. Li, "Inorganic samples with two magnetic phases," in *Magneto-Optical Kerr Effect Spectroscopy Study of Ferromagnetic Metal/Organic Heterostructures,* PhD Thesis (Technische Universität Chemnitz, Chemnitz, 2010).
20. O. Hellwig, J. K. Bosworth, E. Dobisz, D. Kercher, T. Hauet, G. Zeltzer, J. D. Risner-Jamtgaard, D. Yaney, and R. Ruiz, "Bit patterned media based on block copolymer directed assembly with narrow magnetic switching field distribution," Appl. Phys. Lett. **96**, 052511 (2010).

1. Introduction

The magneto-optical Kerr effect (MOKE) is widely used in research and industrial applications to assess the magnetic properties of materials, since in a first-order approximation the MOKE signal is proportional to the magnetization of the studied material (see *e.g.* [1]). While MOKE spectroscopy has been used to characterize the magnetism and the chemical composition of elemental [2] and alloy [3] ferromagnetic layers for some time, it was only recently demonstrated to be applicable to the study of organic semiconductors [4,5]. Even when the organic semiconductor itself does not exhibit a strong MOKE signal, its optical properties influence the magneto-optical response of a ferromagnetic substrate [6,7] or ferromagnetic top layer [8]. When appropriate conditions for multiple internal reflections at the metal/organic interface are met, the magnitude and shape of the MOKE spectra can be tuned by changing the film thickness [8]. Similar effects were observed when using inorganic optical coatings (see *e.g.* [9] and references therein) and can be exploited for enhancing the MOKE signal of nanomagnets (*e.g.* [10]) or for improving the design of magneto-optical storage media [6,7]. This can also affect the lineshape of MOKE hysteresis loops, leading to discrepancies compared to SQUID (M-H) hysteresis loops, leading to so-called "optical artefacts" or "anomalous" shapes of MOKE hysteresis loops. The interpretation of the MOKE spectra of complex systems needs to be sustained by numerical calculations, see *e.g.* [4,8,9,11] and references therein. As input parameters, both the diagonal and off-diagonal elements of the dielectric tensor (or the optical constants and the magneto-optical Voigt constant) of the layers and the substrate are required. The agreement between the calculated and experimental spectra depends strongly on the applicability of the optical model to the real system. While the measured spectra of heterostructures with nearly flat interfaces are described well by the simulated spectra, the divergence between the measured and calculated spectra is significant for polycrystalline films [8]. Here we demonstrate, using the example of a metal/organic heterostructure (Ni/rubrene), that spectroscopic, field-dependent MOKE measurements can be used to identify the presence of more than one magnetic component in the system and to separate their respective contributions to the total magneto-optical signal.

#208434 - $15.00 USD Received 19 Mar 2014; revised 8 May 2014; accepted 24 Jun 2014; published 23 Jul 2014
(C) 2014 OSA

2. Sample preparation and characterization

2.1 Sample preparation

With its high charge carrier mobility [12] and long spin relaxation times [13], rubrene ($C_{42}H_{28}$) has been thoroughly investigated in the view of its integration as an organic semiconductor material in electronic and spintronics devices. For our study, rubrene films are used as nanopatterned templates for the growth of a thin Ni layer. Depending on the substrate surface, temperature, and evaporation rate, the growth mode of rubrene varies from well separated molecular islands to smooth, continuous films [8,14,15]. In this work, we use rubrene films with a nominal thickness of 15 nm, which were deposited at room temperature by thermal evaporation in ultra-high vacuum using an evaporation rate of (0.11 ± 0.02) nm/min on naturally oxidized Si(111) substrates. With this approach, well separated rubrene islands with lateral sizes of about 100 nm to 200 nm are formed [8].

When a 14-nm-thick Ni film is deposited by electron beam evaporation with a rate of (0.26 ± 0.03) nm/min, the morphology of the Ni layer follows that of the rubrene underneath [8]. The islands in the Ni/rubrene heterostructure consist of rubrene capped with a Ni layer, while the Ni film formed between the islands is directly deposited on the Si substrate. As shown by Li *et al*. [8], the top Ni layer can be oxidized partially when the sample is exposed to air. A typical atomic force microscopy (AFM) image of a Ni(14 nm)/rubrene(15 nm) bilayer sample is shown in Fig. 1(a).

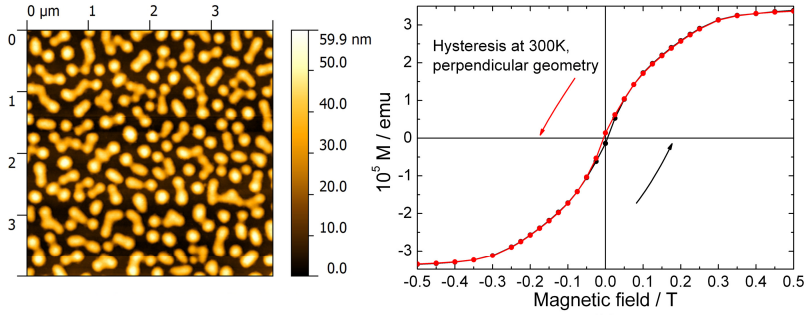

Fig. 1. (a) AFM image and (b) SQUID (M-H) hysteresis loop of a Ni(14 nm)/rubrene(15 nm) bilayer measured in perpendicular geometry at room temperature.

2.2 SQUID magnetometry

The magnetic properties of this Ni/rubrene bilayer were investigated by MOKE spectroscopy and SQUID magnetometry.

For Ni films grown on preoxidized Cu(110)-(2x1)-O substrates with a thickness larger than 11 nm (40 ML) an in-plane magnetization was reported [2]. In our case, the Ni films grown on naturally oxidized Si(111) substrates will not be substantially strained. The shape anisotropy is thus expected to favor an in-plane magnetization even for film thicknesses lower than the critical thickness reported in [2], with a small out-of-plane component that might be caused by film roughness and waviness. Indeed, SQUID (M-H) hysteresis loops recorded at room temperature (RT) with the magnetic field direction parallel to the sample surface as well as perpendicular to it show that the easy magnetization axis of the Ni film lies in the sample surface plane. Figure 1(b) shows the (M-H) loops recorded in perpendicular geometry for the sake of comparison with polar MOKE magnetometry measurements. The perpendicular SQUID (M-H) hysteresis loops exhibit a S-shape with a small coercive field ($\mu_0 H_c = 5.30$ mT) and remanence magnetization (M_r) in agreement with the fact that the easy magnetization axis of the Ni film lies in the sample surface plane. However, a superparamagnetic contribution from Ni diffusing into the rubrene islands cannot be excluded.

#208434 - $15.00 USD Received 19 Mar 2014; revised 8 May 2014; accepted 24 Jun 2014; published 23 Jul 2014
(C) 2014 OSA

2.3 MOKE magnetometry

The MOKE setup is home-built following the design by Herrmann *et al.* [2] and allows acquiring MOKE spectra in the energy range from 1.75 eV to 5 eV and in an applied magnetic field up to 1.7 T. All MOKE measurements presented in this paper were carried out *ex situ* in ambient condition at RT. In the polar MOKE setup the magnetic field is normal to the sample surface and the incidence angle is ~ 1.3°. The MOKE hysteresis probed by Kerr rotation at a photon energy of 4.72 eV and measured at RT in polar geometry (similar conditions as in SQUID),

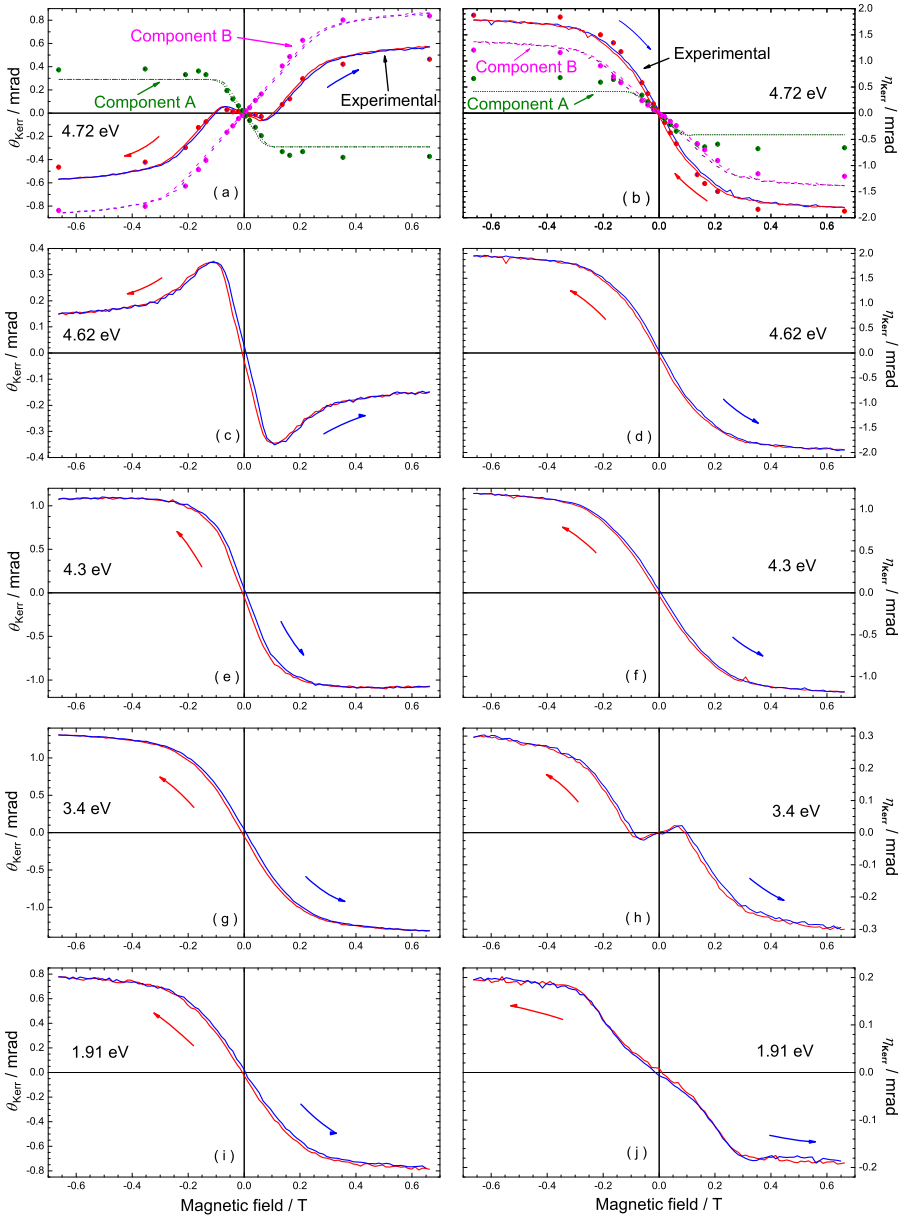

Fig. 2. (a-j) Hysteresis measured by polar MOKE at RT and at various photon energies. The left and right panels show the real part (rotation) and the imaginary part (ellipticity), respectively, of the complex MOKE signal.

#208434 - $15.00 USD Received 19 Mar 2014; revised 8 May 2014; accepted 24 Jun 2014; published 23 Jul 2014
(C) 2014 OSA

shows a kink at a magnetic field strength of about 70 mT (Fig. 2(a)). The MOKE hysteresis of the Kerr ellipticity at the same photon energy, 4.72 eV, however, has a similar shape as measured by SQUID, as it can be seen in Fig. 2(b). In the following, we will show that the energy dependent hysteresis lineshape is a purely optical effect and can be reproduced when considering a linear combination of the spectra of two different magnetic components.

3. Two magnetic components

3.1 Model

Due to the laterally inhomogeneous structure, one possible explanation is that the Ni layer grown on top and between rubrene islands has different magnetic properties. Even though the SQUID, which measures the integral magnetic moments from Ni on and between the rubrene islands, is not able to distinguish the difference in magnetic properties between these two Ni areas, MOKE turns out to be very sensitive to probe it. Such discrepancies between MOKE and SQUID hysteresis loop shapes were already reported in literature (see *e.g.* [16]).

The measured spectroscopic MOKE signal $\theta(\omega, H)$ is a function of photon energy ($E = \hbar\omega$) and applied magnetic field H and can be written as the sum of spectra of different magnetic components. In a first approach, we assume the presence of two components, which should be related to the Ni layer between the rubrene islands (component A) and on top of rubrene islands (component B). The measured MOKE spectra can then be written as a linear combination of the spectra of the two components at each applied magnetic field strength:

$$\theta(\omega, \mathrm{H}) = a \cdot \theta_A(\omega, \mathrm{H}) + b \cdot \theta_B(\omega, \mathrm{H}) , \qquad (1)$$

where a and b are the magnetic field dependent weighting coefficients.

3.2 Field-dependent MOKE spectra

As the two magnetic components are expected to saturate at different applied fields, the complex MOKE spectra were recorded as a function of applied magnetic field.

The features observed in the Kerr rotation spectra in Fig. 3(a) undergo a red shift and the spectral shape changes gradually with increasing magnetic field. The relative height between features around 3.6 eV and 4.3 eV and the slope of the spectrum for photon energies above 4.5 eV change with the magnetic field. The spectral features in the Kerr ellipticity also exhibit a red shift and a relative height change of the two features around 3.8 eV and 4.7 eV as shown in Fig. 3(b). The insets in Fig. 3 show the regions where the Kerr rotation and the Kerr ellipticity cross the zero line, *i.e.* change their sign.

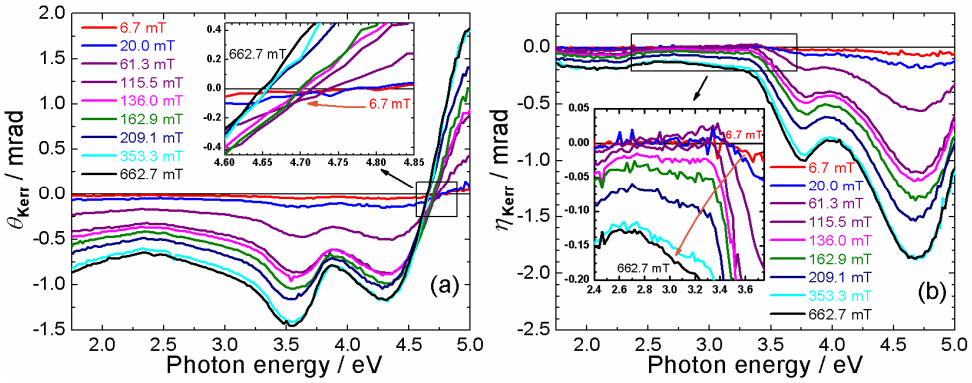

Fig. 3. MOKE spectra of the Ni(14 nm)/rubrene(15 nm) bilayer at different applied magnetic field strengths. (a) Spectra of the Kerr rotation. The inset shows the spectra near the zero-crossing point. (b) Magnetic field dependent Kerr ellipticity spectra. The inset shows the enlarged spectral range from 2.4 eV to 3.75 eV.

#208434 - $15.00 USD Received 19 Mar 2014; revised 8 May 2014; accepted 24 Jun 2014; published 23 Jul 2014
(C) 2014 OSA

3.3 Separation of the magneto-optical contribution of the two components

In a second step, the complex MOKE spectra of the two components ($\theta_A(\omega,\mathrm{H})$ and $\theta_B(\omega,\mathrm{H})$) have to be extracted from the measured MOKE spectra.

Let us consider the MOKE spectra recorded at 126.03 mT and 209.13 mT. In both cases, the MOKE signal of component A is already saturated, while the signal of component B is still increasing linearly with applied field (Fig. 2(a)):

$$\theta_B(\omega,\mathrm{H}) = \mathrm{H}\cdot\theta_{BI}(\omega), \tag{2}$$

where $\mu_0\,\mathrm{H}$ is the applied magnetic field in units of mT, and $\theta_{BI}(\omega)$ is the MOKE spectrum of component B at $\mu_0\mathrm{H} = 1$ mT.

The measured Kerr rotation spectra can be written as:

$$\theta(\omega,126.03mT) = \theta_A(\omega,H_s) + 126.03\cdot\theta_{BI}(\omega) \tag{3}$$

and

$$\theta(\omega,209.13mT) = \theta_A(\omega,H_s) + 209.13\cdot\theta_{BI}(\omega) \tag{4}$$

Here $\mu_0\,\mathrm{H}_S$ is the magnetic field where the magnetization of component A is saturating. From Eqs. (3) and (4) the two unknown quantities, $\theta_A(\omega,H_s)$ and $\theta_{BI}(\omega)$, can be calculated. With the knowledge of $\theta_{BI}(\omega)$ and $\theta_A(\omega,H_s)$, we can then calculate $\theta(\omega,\mathrm{H})$ at any applied field above the saturation point of component A, *e.g.* at 662.7 mT.

The obtained real and imaginary parts of the complex Kerr signal spectra of components A and B are shown in Figs. 4(a) and 4(b), exemplary for a magnetic field strength of 662.7 mT. For comparison, the MOKE spectra taken at remanence (zero applied field) are also presented. The spectrum of component A has a very similar lineshape to the spectrum recorded in remanence.

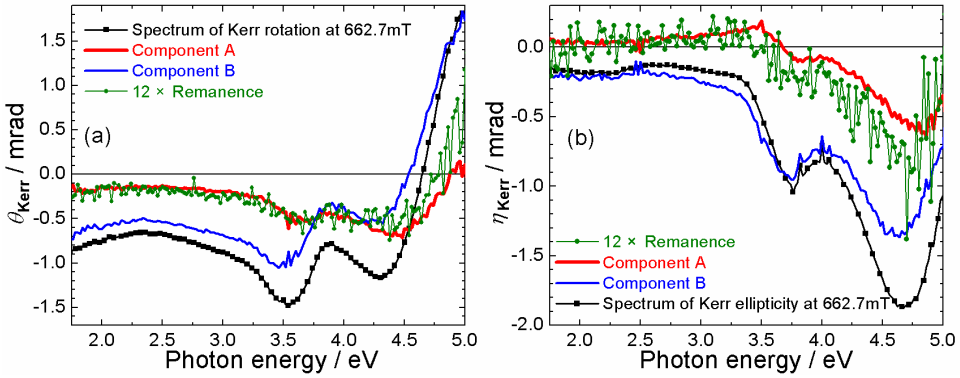

Fig. 4. Complex MOKE rotation spectra of a Ni(14 nm)/rubrene(15 nm) bilayer recorded at 662.7 mT (line plus squares) compared to the spectrum recorded in remanence (line plus circles, enlarged by 12 times) and to the calculated spectra of component A (bold red line) and component B (thin blue line). Figure (a) displays the real part and figure (b) shows the imaginary part of the complex Kerr signal.

In order to test the reliability of the procedure described above, we calculated the MOKE spectra as a weighted sum of the component A and component B spectra (at 136.03 mT) for several magnetic field strengths and compared them to the experimental ones. These are represented by symbols and lines, respectively, in Fig. 5. The weighting coefficients of spectra of component A and component B (at 136.03 mT) are given in the Table 1. All calculated spectra match excellently the experimental spectra.

#208434 - $15.00 USD Received 19 Mar 2014; revised 8 May 2014; accepted 24 Jun 2014; published 23 Jul 2014
(C) 2014 OSA

Table 1. Weighting coefficients used for simulating the experimental MOKE spectra shown in Fig. 5

	6.66 mT	19.99 mT	136.03 mT	162.91 mT	209.13 mT	662.67 mT
Component A	0.064	0.188	1.000	1.093	0.999	1.124
Component B	0.049	0.114	1.000	1.198	1.550	2.067

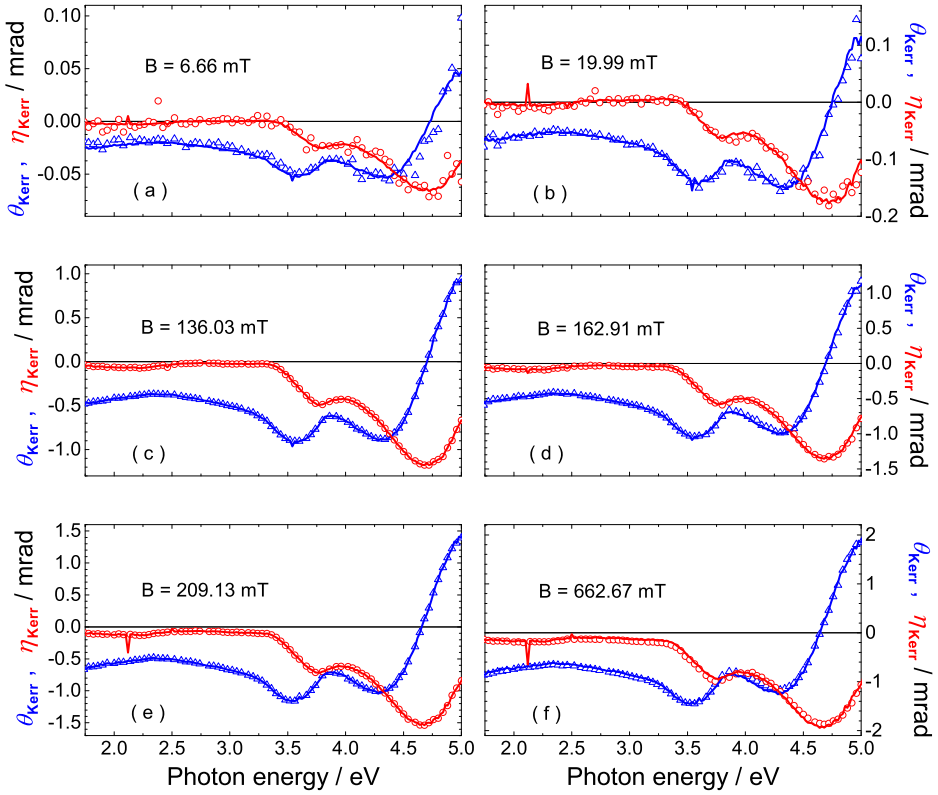

Fig. 5. Complex Kerr rotation spectra for the magnetic field strength of (a) 6.66 mT, (b) 19.99 mT, (c) 136.03 mT, (d) 162.91 mT, (e) 209.13 mT, and (f) 662.67 mT. The symbols correspond to the experimental data and the solid lines to the simulated spectra. Blue and red represent the real and imaginary parts, respectively.

4. Interpretation

4.1 Explanation of the MOKE hysteresis

Knowing the MOKE spectra of the components A and B, the hystereses shown in Figs. 2(a) and 2(b) can easily be explained. At 4.72 eV, near the zero-crossing point of the MOKE rotation spectrum, cf. Fig. 3(a), the Kerr rotation value of component A is negative while that of component B is positive. At low magnetic fields the contribution from component A is dominant, so the total MOKE signal is negative. Above 70 mT, the MOKE signal from component A is saturated while the contribution of component B continues to increase. As a consequence, a change in slope occurs in the hysteresis, providing the "anomalous" behavior shown in Fig. 2(a). The dots in Fig. 2(a) correspond to the calculated MOKE signal displayed in Fig. 5 based on a linear combination of the spectra of component A and B (shown in Fig. 4) at a photon energy of 4.72 eV. The evolution of the Kerr ellipticity at 4.72 eV with applied magnetic field can be explained considering that the imaginary part of the Kerr spectra of both components have a negative sign, cf. Figs. 2(b) and 3(b).

#208434 - $15.00 USD Received 19 Mar 2014; revised 8 May 2014; accepted 24 Jun 2014; published 23 Jul 2014
(C) 2014 OSA

With the knowledge of the MOKE spectra of components A and B, we can predict the behaviour of the MOKE hysteresis at various photon energies. For example, at 1.91 eV, which is close to the energy of the HeNe laser often used as a light source in many MOKE magnetometry setups, the sign of the Kerr ellipticity signal does not change except around zero magnetic field as seen in Figs. 2(j) and 3(b). Here the component A has a small amplitude and hence its contribution to the Kerr ellipticity is relatively small. However, the opposite values in the imaginary part of the MOKE signal from component A and component B lead to a slope change in the hysteresis loop, cf. Fig. 2(j). The turning point of the slope is also around 70 mT, where the signal of component A saturates.

4.2 Discussion of the origins of the two components

The MOKE spectrum of component A is very similar to that of the spectrum recorded at remanence, see Fig. 4. Furthermore, component A reaches saturation at lower applied magnetic field than component B. These two facts are consistent with the assumption that component A stems from the Ni film located between the islands, which can couple magnetically better than the separated Ni caps on top of the rubrene islands. A partial oxidation of the Ni layer cannot be excluded. However, previous studies of Ni films deposited onto rubrene layers showed that only a small fraction (below 1 nm) of the Ni will be oxidized [8]. While NiO itself exhibits no MOKE signal, its refractive index might contribute to a modulation of the MOKE spectra. However, MOKE spectra modelling (not shown here) using the optical multi-layer model described in reference [8] showed that a thickness below 1 nm is too low to bring a significant contribution to the MOKE spectra of component A or component B. The presence of an antiferromagnetic NiO layer that couples to the ferromagnetic Ni layer might shift the magnetic hysteresis loops via the exchange bias effect. However, in our system no fingerprint of the exchange bias effect at least at room temperature was observed, cf. Fig. 2.

To support the hypothesis that component B stems from the capping layer of Ni on top of the islands, we carried out experimental measurements on a sample with the same nominal structure, Ni(14 nm)/rubrene(15 nm), but having a different morphology. In this case, the rubrene layer was deposited at a higher evaporation rate (10 nm/min). The morphology of the resulting rubrene layer and of the Ni/rubrene heterostructure was probed by AFM. Figure 6(a) shows that the heterostructure is characterized by closely packed islands. This fact hinders the formation of a continuous Ni film between the rubrene islands directly on the SiO_2/Si substrate. Hence, for this sample, the measured MOKE spectra are expected to be dominated by the signal of the Ni on top of rubrene. Indeed, the measured MOKE spectrum of this sample is very similar in lineshape to that of component B, as can be seen by a direct comparison of the spectra displayed in Fig. 6(b). The MOKE hysteresis and field-dependent MOKE spectroscopic measurements on this sample clearly show the existence of only one magnetic component, confirming our hypothesis, regarding the origin of component B.

As often observed when a metal is deposited onto organic films [17], Ni could diffuse inside the rubrene islands and form small particles. For such kind of small particles, the lack of saturation even at large magnetic fields could occur due to spin frustration at the surface [18]. The presence of Ni particles inside the rubrene islands might be the reason why the magnetization of component B is hard to saturate even at much higher applied fields as compared to component A. For the validation of this hypothesis further temperature dependent magnetometry and X-ray photoemission studies will be necessary. However, independently of the origin of this magnetic component, its distinct MOKE spectrum provides a suitable contribution to the total magneto-optical activity, which allows the proof-of-concept for our magnetic-field dependent approach to separate the contributions in our heterostructure.

#208434 - $15.00 USD Received 19 Mar 2014; revised 8 May 2014; accepted 24 Jun 2014; published 23 Jul 2014
(C) 2014 OSA

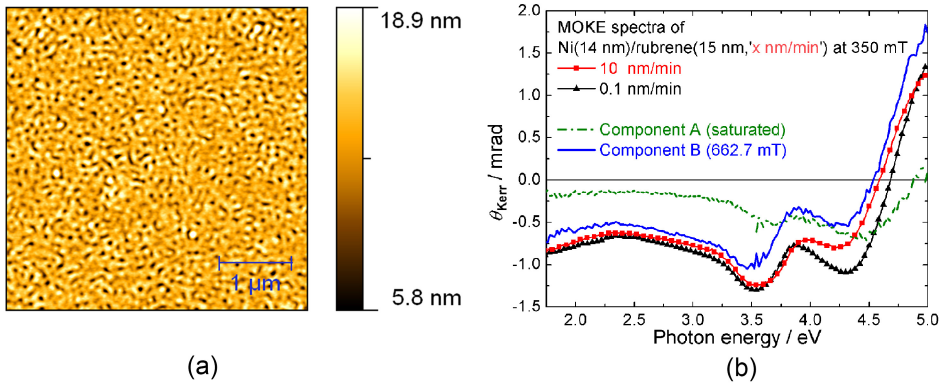

Fig. 6. (a) AFM image of a Ni(14 nm)/rubrene(15 nm) bilayer for which rubrene was deposited with a rate of 10 nm/min. (b) The MOKE spectra at 350 mT of the two Ni(14 nm)/rubrene(15 nm) bilayers for which rubrene were deposited with 10 nm/min and 0.1 nm/min. The MOKE spectra of components A and B are also plotted for comparison.

5. Model generalization

In general, if a lateral inhomogeneous magnetic system has two or several types of de-coupled magnetic sub-structures, the magnetic components can be separated using MOKE spectroscopy under the following considerations:

(1) each type of the sub-structure has unique magnetic properties due to its special composition, anisotropy, size/surface effect, oxidation *etc.*, or

(2) the light experiences multiple reflections and transmissions in the nano-scale structures. Thus the difference in thickness, composition, and/or morphology can lead to different MOKE spectral shape for each sub-structure; and

(3) by the choice of appropriate energy positions (*e.g.* in the vicinity of the MOKE spectrum zero-crossing point) the difference in magnetic properties can be evidenced by MOKE hysteresis measurement as exemplified in our study.

The method described in this work can be extended to a wide range of magnetic sub-structures with various sizes and morphologies. Besides the Ni/rubrene bilayes, we performed this analysis for Ni films grown on nanostructured silicon substrates [19]. Similar "anomalous" MOKE hysteresis loops were also reported for other purely inorganic samples [16,20]. For example, Hellwig *et al.* observed anomalous MOKE hysteresis for Co/Pd multilayers in bit patterned media, where Co/Pd on pillars and trenches are de-coupled from each other [20]. Besides the lateral inhomogeneous nanostructures, sub-structures of flat layers at different depths were also reported to show more magnetic components [1]. In this case, the phase shift technique was applied in order to distinguish between the signals of the different buried layers [1].

Similar observations were also reported in a film composed of $BiFeO_3$ and $CoFe_2O_4$ domains [16]. Postava *et al.* proposed a method to extract the hysteresis of two magnetic components from the complex MOKE hysteresis loop recorded at a single photon energy, based on the knowledge of the optical constants of the two constituent materials [16]. The main advantage of our spectroscopic approach is that it does not require the *a priori* knowledge of the optical constants.

6. Summary

In conclusion, using the example of Ni/rubrene bilayer, we demonstrated that polar field-dependent MOKE spectroscopy is a very powerful tool to separate the magneto-optical

#208434 - $15.00 USD Received 19 Mar 2014; revised 8 May 2014; accepted 24 Jun 2014; published 23 Jul 2014
(C) 2014 OSA

activity of two magnetic components in laterally inhomogeneous magnetic structures. The field-dependent spectral shape of the complex Kerr rotation angle and the shape of the "anomalous" hysteresis loops measured by MOKE can be consistently reproduced by calculating numerically the linear combination of the spectra of two magnetic components. Based on the spectral shape and the saturation field, these spectra could be attributed to Ni on top and between the rubrene islands. This finding demonstrates the capabilities of MOKE magnetometry in combination with MOKE spectroscopy and its advantage over non-optical magnetometry methods such as SQUID. The great advantage of the linear combination method described in this work lies in the richness of information related to the chemical and structural properties, which can be extracted from the spectra of the two (or more) magnetic components. This opens a path for the use of field-dependent MOKE spectroscopy both in applications and fundamental studies.

Acknowledgments

The German Research Foundation (DFG project FOR 1154) and the Scientific Research Foundation of the Civil Aviation University of China (project 2012QD15X) are gratefully acknowledged for financial support. We are grateful to R. Magerle (TU Chemnitz, Germany) for providing access to the AFM facilities. The publication costs of this article were funded by the German Research Foundation/DFG (Geschäftszeichen INST 270/219-1) and the Chemnitz University of Technology in the funding programme Open Access Publishing.

#208434 - $15.00 USD Received 19 Mar 2014; revised 8 May 2014; accepted 24 Jun 2014; published 23 Jul 2014
(C) 2014 OSA

137.250.102.73 {ts '2019-11-20 01:23:39'}